

Predicting LPBF Ti-6Al-4V Microstructure via Multi-Modal In-Situ Process Monitoring

Ankita Roy^a, Dana Drake^b, Rajiv Mishra^a, Yash Parikh^b

^aDepartment of Material Science and Engineering, University of North Texas, Denton, Texas
76207, USA

^bEOS of North America, Inc., 3813 Helios Way – Suite B 298, Pflugerville, Texas 78660, USA

Abstract

Accelerating qualification of laser powder bed fusion (LPBF) components for serial production requires innovative approaches beyond extensive empirical testing. In-situ process monitoring (ISPM) offers a powerful means to detect and characterize process deviations in real-time, providing valuable insights into process stability. By examining identical parts and parts having systematic cross-section variations printed using Ti-6Al-4V alloy, we first aim to understand the printability domain influencing in-situ sensor signals to minimize printing defects and maximize density. Next, we investigate correlation between these in-situ signatures and resulting microstructural characteristics, which are affected by thermal history, depending on part dimensions. Integration of Closed Loop Control (CLC) for real-time thermal management and anomaly mitigation will also be considered, which can impact both process stability and resulting microstructure. The goal is to establish a data-driven framework that leverages ISPM, potentially integrated with machine learning (ML), to predict microstructural features and mechanical properties, thereby reducing reliance on time-consuming and resource-intensive post-build testing and accelerating qualifications.

Introduction

Laser Powder Bed Fusion (LPBF) enables the production of complex parts with less material waste and faster turnaround when compared with conventional manufacturing techniques. However, LPBF widespread adaptability can only be fully leveraged if the processes of qualification and standardization¹⁻³ are accelerated and repeatable^{4,5}. Typically, part qualification involves two major steps: first, ensuring the fabrication of parts with minimal pores or cracks to achieve consistent mechanical performance (*e.g.*, strength and elongation), and second, establishing uniform microstructure across builds to mitigate issues such as anisotropy, grain size variation, precipitate formation, elemental segregation, lath morphology, and heat treatment sensitivity⁶. This enables repeatable and reproducible LPBF parts which are machine agnostic.

Recent advancements in ISPM technologies such as those shown in Figures 1 (a, b), have enabled real-time capture of key signals during printing that correlate strongly with defect formation and microstructural variation. For example, the Powder Bed Camera which is a simple optical camera working in the visible light range tracks the uniformity of spreading powder. It can detect defects such as recoater streaking, powder short-feeding as well as part warpages. Optical Tomography

(OT) is an off-axis mounted sCMOS camera that records heat accumulation in geometrically complex regions (*e.g.*, up-skin/down-skin). It measures the emitted near IR radiation from hot build surface using Si photodiodes and displays integrated intensities. These are typically called Gray Values (GVs) and based on 8-bit or 16-bit configurations can vary from 0-256 and 0-65,535 (where lower limit indicates no emittance). Melt Pool Monitoring (MPM) captures melt pool temperature fluctuations using fast photodiodes and co-axial cameras often calibrated to temperatures. These sensor modalities, integrated within the EOS Smart Monitoring suite, enable a higher degree of process control, offering the potential to stabilize final part properties.

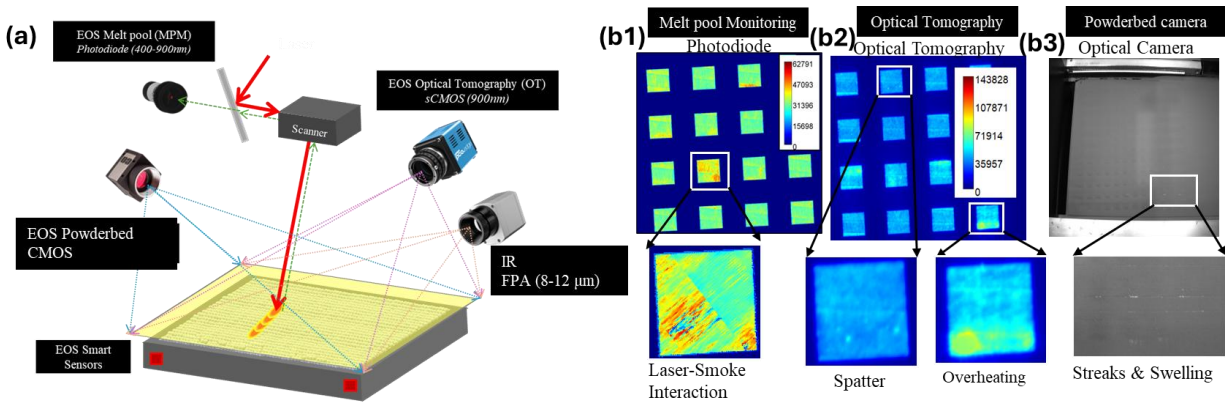
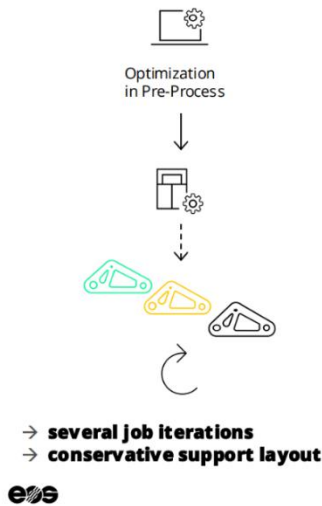


Figure 1: (a) Signals from in-situ process monitoring (b1-b3) Different modalities for in-situ defect detection using EOS Smart Monitoring suite (Melt Pool Monitoring, Exposure OT, Powder bed camera)

The existing state-of-art entails detection of anomalies in each layer leading to defects in the overall build using ISPMs. Detection of out-of-bound signals and their correlation to the defects in the final build is followed by correction in processing parameters in the following runs associated with the defects and recording the improvement in the print quality. This procedure of detection and elimination is called feed-forward control (shown in Figure 2 (a)). This system, although is high effective, accepted and easy to implement, is very cost- and time-intensive.

A recent innovation- Smartfusion (shown in Figure 2 (b)) is a feature offered by EOS that implements closed-loop control (CLC)⁷⁻⁹ by dynamically adjusting the mean Grey Value (\overline{GV}) for each print layer based on OT data. It is a PID controller that enables run-time correction of laser-power based on the threshold GV from previous 5-10 layers, thereby acting as a feedback control loop, correcting defects on the g. By controlling mean \overline{GV} , the system modulates layer-wise heat input, thereby mitigating pore/crack formation while influencing the evolving microstructure. This is particularly crucial for alloys like Ti-6Al-4V, widely used in aerospace and defense applications due to their high specific strength. As an $\alpha+\beta$ titanium alloy¹⁰, Ti-6Al-4V exhibits microstructural variability in α -lath size, β -phase distribution, and prior β -grain morphology, which are all sensitive to the local thermal history and can be further tuned via post-build heat treatment^{3,11,12}.

(a) Conventional:
Feed Forward
Control



(b) Smart Fusion:
Feed-Back Control

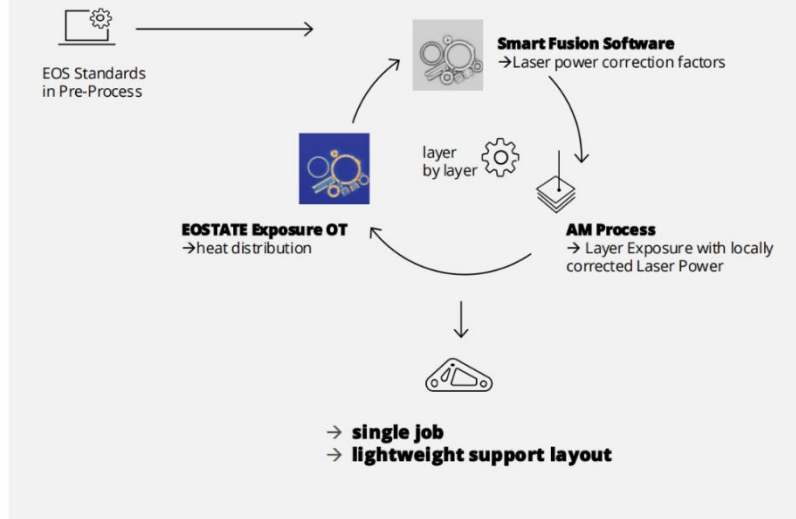


Figure 2: (a) Conventional feed forward control is where process parameters are fed forward and multiple job iterations are required to modify a certain anomaly (b) Closed-loop control (CLC) technique using EOS Smart-fusion technology uses a feedback loop to control the heat distribution based on the sensor feedback and corrects any anomaly on-the-fly.

The primary aim of this study is to investigate the effect of CLC via SmartFusion on the microstructural evolution and mechanical response of LPBF builds. For this purpose, a build layout was designed, and samples were printed both with and without CLC-printed using Ti-6Al-4V. OT data from a baseline build was analyzed to extract layer-wise mean \overline{GV} , which was then used as input for the CLC-enabled build. Microstructural characterization revealed that both α -lath and prior β -grain morphology were largely preserved across builds with and without CLC. However, a significant reduction in hardness variability was observed in the CLC-enabled parts. This was attributed to lower residual stress and reduced dislocation density, emphasizing SmartFusion's effectiveness in enhancing process stability and enabling data-informed, real-time control for digital part qualification.

Materials and Methods

The experiments were conducted on Electro Optical Systems (EOS GmbH) M290 system using Ti-6Al-4V (Grade 5) powder feedstock (Table 1) using processing parameters (Table 2)^{12, 13}.

Table 1: Chemical composition of Ti-6Al-4V (Grade 5) powder as per EOS specifications.

	Ti	Al	V	O	N	C	Fe
Ti-6Al-4V	Bal.	6.5	4.05	0.16	0.018	0.015	0.20

Table 2: EOS M290 process parameters used to fabricate Ti-6Al-4V samples.

Laser Power (W)	Scan Speed (mm/s)	Hatch Distance (μm)	Layer Thickness (μm)	VED (J/mm^3)
340	1250	120	60	38

To characterize microstructural features, optical microscopy at multiple magnifications was carried out along the plane parallel to the direction of the build. For capturing optical micrographs and topographical information about lath size, the samples were lightly etched with Kroll's solution after polishing using $0.02 \mu\text{m}$ colloidal silica solution. Unetched samples were used for electron backscattered diffraction (EBSD) mapping. Optical images were captured using Keyence VHX-7100 Digital microscope while EBSD scans were recorded with attached Hikari EBSD detector at a voltage of 30 kV and 15 nA current and post-processed using TSL OIM 8 software at the University of North Texas.

Two sets of builds with similar layouts (142 units) were chosen for this study shown in Figure 3 (a-d), with the first set printed without CLC and the second set with CLC. Figure 3 (a, b) shows the dimensions of each unit and printed layout of all these units within the baseline builds. The sample geometry was chosen such that the variation in OT signals across variations in sample geometries (cuboidal, cylindrical, conical) can be recorded. Figure 3 (c) shows the mean \overline{GV} , of each unit averaged over all the layers from bottom to top. The first and second set in Figure 3 (d1, d2) respectively showed OT signals from the baseline builds consisting of all bullet-shaped specimens printed without-CLC and with-CLC.

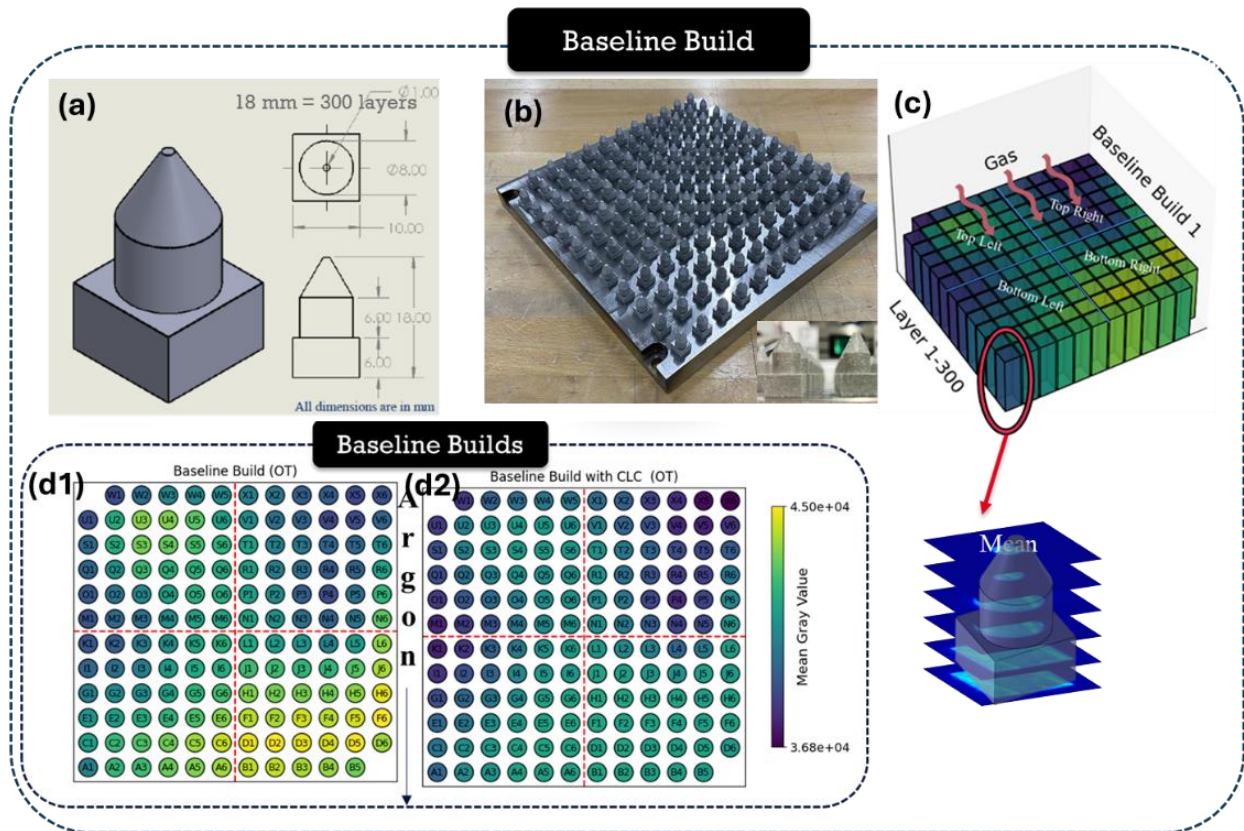


Figure 3: (a) Dimensions and projections of each unit (b) Layout of baseline build (for both with and without CLC) (c) Mean \overline{GV} , calculation for each unit (d1, d2) OT signals from baseline builds with bullet-like specimens printed with same layout with- and without-CLC

Results and discussion

Figure 4 presents a comprehensive analysis of the microstructure from both the builds without-CLC (Figures 4 (a1 - a4)) and with-CLC (Figures 4 (b1 - b4)). Figure 4 (a1, b1) shows the optical micrographs at light-field mode at low magnification showing that both builds are devoid of any cracks or pores while figures 4 (a2 and b2) show higher magnification images in dark-field optical mode to highlight the laths of both the builds along the build direction (X-Z plane) for the cylindrical region corresponding to 6 mm -12 mm of the build height. The comparative mean \overline{GV} , from the OT signals of the corresponding layers is shown in Figure 4 (c). While Figure 4 (d) shows comparative parent grain reconstructed prior β - grains sizes.

Figures 4 (a2, b2) highlight epitaxial growth of the β - grains across multiple deposited layers (shown by 1,2,3 as number of layers) in the dark-field mode of an optical micrograph. The etching reveals the as-deposited layers as well as the boundaries of the prior beta-grains. Multiple α - laths growing within one β grain are observed in the optical micrograph. These laths are clearly shown and orientation is mapped using the IPF using an EBSD detector. Next, with the help of prior parent β - grain reconstruction is carried out using $\langle 11\bar{2}0 \rangle$ matching with $\langle 1\bar{1}1 \rangle$. It was

observed in Figure 4 (d) that the prior β -grain size/area (both along major and minor axis) was almost similar in both cases

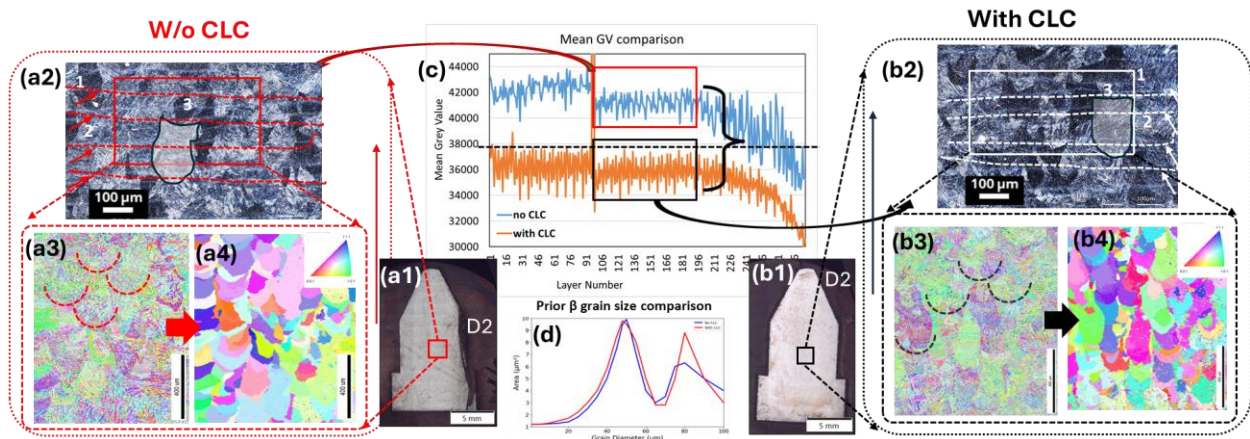


Figure 4: (a1-a4) Without-CLC, and (b1-b4) With-CLC, (a1, b1) Optical low magnification light-field montage of the printed X-Z cross-section along the build direction. (a2, b2) Dark-field images showing α laths within β grains. (a3, b3) Low magnification orientation image used for parent β grain (a4, b4) Reconstructed parent β grains (c) OT signal comparison of both the builds (d) Prior β - grain size mapping for builds with- and without-CLC.

Figures 5 (a1, b1) show comparative analysis in lath size and orientation in both the builds while figures 5 (a2, b2) show comparison in α and β -phase fraction. Although no considerable variation in lath size distribution or phase was observed in the cylindrical region, higher mean hardness with higher standard deviation value was observed for samples without-CLC in Figure 5 (c).

Hardness variation recorded along the build height for both the samples showed a mean hardness of 395 ± 6 HV for the sample with-CLC and 405 ± 10 HV for the sample without-CLC.

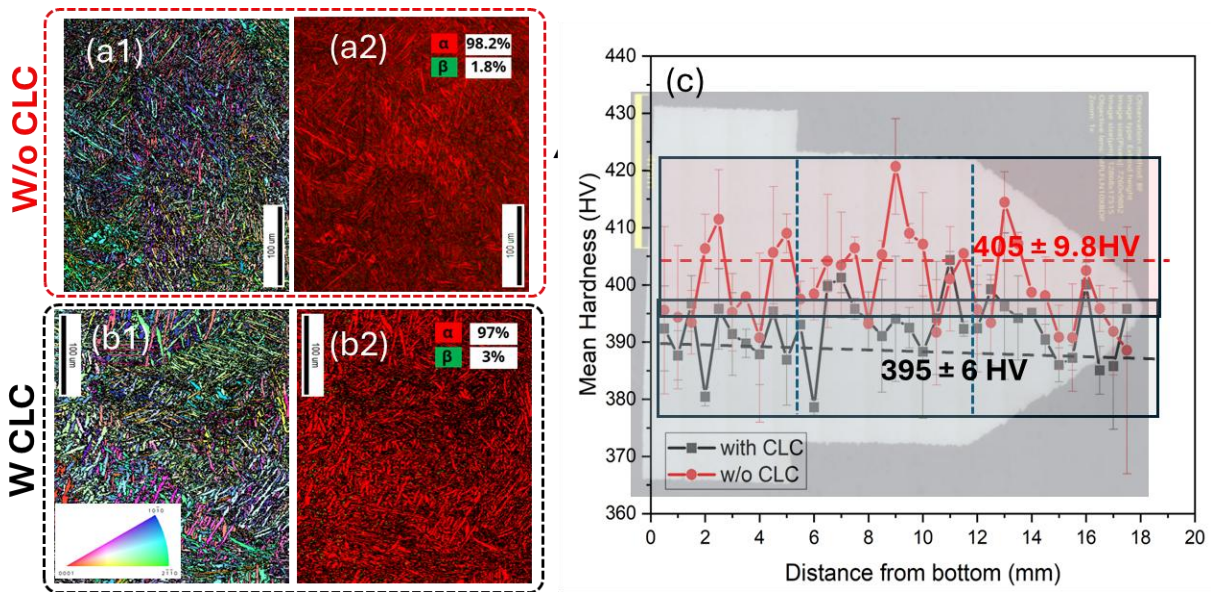


Figure 5: (a1, b1) IPF image showing size and orientation of α -laths for without and with CLC respectively (a2, b2) Phase map showing relative volume fractions of α and β phase fractions respectively (c) Shows hardness variation within the build from bottom to top.

Variation in hardness in the two samples despite the similar α , β - grain sizes and final phase fractions indicates the presence of higher residual stresses and dislocation density in the samples without CLC due to variation in heat input in different layers. The results highlight an important aspect of the samples printed using CLC. The microstructural analysis reveals that no abnormal grain growth is observed on using CLC and the grain size is controlled in the similar range as without-CLC, however, the residual stress is controlled within closed limits. This marks an important positive step towards qualification of builds.

Conclusion

This study demonstrates that in-situ process monitoring signals like Optical Tomography (OT), can serve as effective indicators for controlling the microstructural and mechanical properties in L-PBF builds. Variations in properties along the build height are primarily attributed to non-uniform heat dissipation across different regions of the built part. OT monitoring captures regions of excessive heat accumulation, and through Closed-Loop Control (CLC) using SmartFusion, localized power input is reduced in these areas. This results in more uniform heat distribution, improved cooling rates, and consequently, a more homogeneous microstructure. Our analysis shows that the samples built without CLC exhibited greater variation in mechanical properties, consistent with the presence of higher residual stresses and microstructural inhomogeneity. In contrast, CLC-enabled builds showed improved consistency, suggesting effective mitigation of localized thermal gradients. These findings highlight the potential of SmartFusion in enabling real-time, data-informed process control, paving the way for digital part

qualification in AM. Future work will extend this investigation to other two geometries, cuboidal and conical regions, to further validate the robustness and scalability of the SmartFusion strategy.

REFERENCES

1. Kawalkar, R., Dubey, H. K. & Lokhande, S. P. A review for advancements in standardization for additive manufacturing. in *Materials Today: Proceedings* vol. 50 1983–1990 (Elsevier Ltd, 2021).
2. Narra, S. P. *et al.* Process qualification of laser powder bed fusion based on processing-defect structure-fatigue properties in Ti-6Al-4V. *J Mater Process Technol* **311**, (2023).
3. Nahr, F. *et al.* Advanced process control in laser-based powder bed fusion—Smart Fusion feedback-loop control as a path to uniform properties for complex structures? *Journal of Materials Research and Technology* **34**, 604–618 (2025).
4. Das, S., Bourell, D. L. & Babu, S. S. Metallic materials for 3D printing. *MRS Bulletin* vol. 41 729–741 Preprint at <https://doi.org/10.1557/mrs.2016.217> (2016).
5. <https://www.eos.info/content/blog/scaling-additive-manufacturing>
6. Roy, A. *et al.* Deciphering mechanical heterogeneity of additively manufactured martensitic steel using high throughput nanoindentation combined with machine learning. *Addit Manuf* **93**, (2024).
7. <https://www.eos.info/content/blog/support-free-smart-fusion>
8. Y. Parikh. *Building Trust, Layer by Layer: How Qualification Ensures Reliable High-Performance AM Parts.* (2024).
9. Yağmur, A., Pääkkönen, I., & Miles Sr, A. (2023). *The Hitchhiker's Guide to Smart Fusion. Whitepaper, EOS GmbH, Germany.*
10. Liu, S. & Shin, Y. C. Additive manufacturing of Ti6Al4V alloy: A review. *Mater Des* **164**, (2019).
11. Wang, Z. *et al.* *Residual Stress Mapping in Inconel 625 Fabricated through Additive Manufacturing: Method for Neutron Diffraction Measurements to Validate Thermomechanical Model Predictions.* (2016).
12. Takase, A., Ishimoto, T., Sugauma, R. & Nakano, T. Surface residual stress and phase stability in unstable β -type Ti–15Mo–5Zr–3Al alloy manufactured by laser and electron beam powder bed fusion technologies. *Addit Manuf* **47**, (2021).
13. <https://www.eos.info/metal-solutions/metal-materials/data-sheets/mds-eos-titanium-ti64-grade-23>